Towards high-quality nitrogen-doped diamond single crystals for X-ray optics

Sergey Shevyrtalov,[a]* Alexander Barannikov,[a] Yurii Palyanov,[b,c] Alexander Khokhryakov,[b,c] Yurii Borzdov,[b] Ilya Sergueev,[d] Sergey Rashchenko[b,c] and Anatoly Snigirev[a]

[a]International Research Center, Coherent X-ray Optics for Megascience Facilities, Immanuel Kant Baltic Federal University, Kaliningrad 236041, Russian Federation, [b]Sobolev Institute of Geology and Mineralogy, Siberian Branch of the Russian Academy of Sciences, Novosibirsk 630090, Russian Federation, [c]Novosibirsk State University, Novosibirsk 630090, Russian Federation, and [d]Deutsches Elektronen-Synchrotron, 22607 Hamburg, Germany. *Correspondence e-mail: shevyrtalov@gmail.com

In this manuscript, characterization of single-crystalline (111) plates prepared from type-Ib diamonds with a nitrogen content of 100–150 ppm by means of high-resolution rocking-curve imaging (RCI) is reported. Contrary to common opinion regarding the intrinsically poor diffraction quality of type-I diamonds, RCI showed the presence of nearly defect-free areas of several millimetres squared in the central part of the diamond plates. The observed broadening of the rocking curves is a result of the cutting and polishing processes, causing strains around the edges of the plates and rare defects. An improvement of the preparation technique will thus allow single-crystalline diamond plates to be made for Laue and Bragg monochromators and beam splitters from type-Ib material with areas large enough to be used as optical elements at fourth-generation synchrotron facilities.

1. Introduction

The emerging new generation of 'diffraction-limited' fourth-generation storage rings based on multi-bend achromat lattice design offers users photon beams of extreme brightness, essential for novel applications that require high coherent flux or nanometre-sized beams (Einfeld *et al.*, 1995). On the other hand, preservation of photon beam phase space and coherent properties becomes an issue that generally cannot be addressed by X-ray optics routinely used at third-generation facilities. Nowadays, Si-based optics elements are widespread at X-ray sources owing to the well established methods of crystal growth and processing, leading to large crystals with a high degree of crystal perfection. However, considering material properties, the preferred material for X-ray optics would be diamond with lower X-ray absorption, lower thermal expansion and much better thermal conductivity. The benefits of using diamond for beam monochromatization at fourth-generation sources include:

(i) Better wavefront preservation by diamond mono-chromators due to smaller thermal 'bumping' compared with silicon devices (a combined effect of low thermal expansion and high thermal conductivity).

(ii) Better angular stability of water-cooled diamond monochromators compared with cryo-cooled silicon devices (Sergueev *et al.*, 2016), essential for preservation of effective source size.
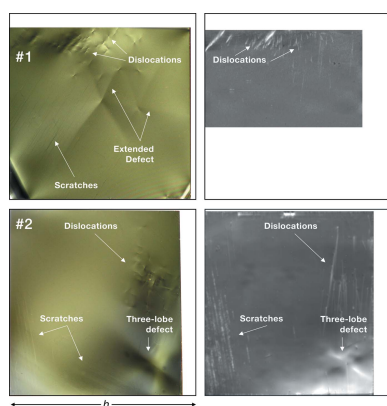
(iii) Small X-ray absorption compared with silicon, allowing for implementation of beam multiplexing schemes (Theveneau *et al.*, 2013).

Diamond crystal plates with (111) surface orientation are of primary importance for diffracting X-ray optics owing to a large intrinsic energy bandwidth of the {111} Bragg reflection ($\Delta E/E = 5.7 \times 10^{-5}$) and the resulting flux of the reflected X-rays compared with those of silicon (Grübel *et al.*, 1996; Yabashi *et al.*, 2007). It is worth noting that at third-generation facilities the Laue geometry is now standard for diamond monochromators in order to minimize beam footprint on crystals made of material with inhomogeneous structure quality. A drawback of such a choice is an inevitable degradation of beam phase space because of intrinsic dispersion of Laue geometry. The corresponding decrease in coherent flux and increase in effective source size is negligible in comparison with effects from electron beam emittance and can be tolerated at third-generation facilities. However, this is definitely not the case for fourth-generation storage rings and X-ray free-electron lasers, where Bragg geometry has to be chosen for coherence-preserving crystal monochromators and beam splitters.

The progress related to the growth of high-quality diamond crystals with at least 2 mm × 2 mm defect- and strain-free surface area is very slow. Large diamond single crystals can be grown by high-pressure and high-temperature (HPHT) techniques with belt-, cubic- or split-sphere-type apparatus (Sumiya & Satoh, 1996; Han *et al.*, 2011; Polyakov *et al.*, 2011). Depending on nitrogen concentration, diamonds are divided into nitrogen-containing type-I, and nitrogen-free type-II, containing less than 1 ppm of nitrogen. Type-I diamonds are further subdivided into type-Ib, containing nitrogen impurity in the form of single substitutional atoms (C-centers), and type-Ia, containing aggregated nitrogen forms (A- and B-centers) (Palyanov *et al.*, 2015).

The monochromators and the beam-splitters demand diamond crystals without dislocations, strains and significant rocking-curve broadening (Burns *et al.*, 2009). According to these requirements diamond Bragg (111) plates with defect-free areas of the order of 5 mm × 5 mm were successfully synthesized and tested in the last decade at LCLS and APS (Stoupin, 2014; Stoupin *et al.*, 2016). Sumiya *et al.* demonstrated the high diffraction quality Bragg (001) and (111) plates cut from the large diamond single crystal up to 12 mm in diameter (Sumiya *et al.*, 2015). These plates were manufactured from synthetic diamonds of type-IIa (nitrogen-free), previously considered to be the only type suitable for growing crystals with large and homogeneous defect-free areas (Shvyd'ko *et al.*, 2017). However, there are only a small number of papers related to the examination of diffraction quality of nitrogen-containing Ia–Ib crystals (Macrander *et al.*, 2005; Hoszowska *et al.*, 2001). Macrander *et al.* showed the strain distribution inside the Ib diamond crystal by measuring the rocking curve shift across the surface (Macrander *et al.*, 2005). The shift varied up to 6 arcsec (29 μrad) could be related to the non-uniform distribution of nitrogen in the crystal. Hoszowska *et al.* performed rocking-curve imaging

(RCI) of (111)-oriented diamond plates doped with nitrogen and observed 1.5 arcsec (7.3 μrad) spread around the crystal attributed to nitrogen impurities (Hoszowska *et al.*, 2001). However, the origin of the lattice imperfection was not clear.

In this work we report the characterization of the diffraction quality of 250 μm-thick type-Ib diamond plates with (111) orientation cut from HPHT grown single crystals that were previously characterized by white-beam topography and the selective-etching method (Khokhryakov *et al.*, 2011). It was found that a dislocation-free volume achieves 58 mm³ and (111)-oriented plates cut from the crystal have a strain-free area of 25 mm². Here, we used X-ray high-energy resolution ($\Delta E/E = 10^{-7}$) RCI from (333) reflections in order to obtain detailed information about the diamond crystal quality. Two measured plates 3 mm × 3 mm in size possess a defect-free area of 1 mm × 2.2 mm and 1 mm × 1.6 mm with a rocking-curve broadening not exceeding 0.6 μrad.

2. Experimental

Synthetic diamond crystals were grown by the temperature gradient method using a high-pressure apparatus of the 'split sphere' type (BARS) and characterized by white-beam topography, selective etching methods and IR absorption spectroscopy (Khokhryakov *et al.*, 2011). The crystals were grown at $P = 5.7$ GPa and $T = 1550°C$ with the use of an $Ni_{0.7}Fe_{0.3}$ alloy as a solvent-catalyst. The crystallization scheme was described in detail in previous work (Khokhryakov *et al.*, 2011; Palyanov *et al.*, 2010). Diamonds grown were octahedral in shape and brownish-yellow in color. An average growth rate was estimated as 39–45 μm h^{-1} for the upper {111} faces of 2.5–3.0 carat crystals.

Two (111)-oriented diamond plates with 3 mm × 3 mm surface areas were cleaved from the outer parts of two single crystals. The plates were mechanically polished from both sides with a slight deviation from the (111) plane. Surface cleanliness was achieved empirically by combining contact pressure and polishing directions. Characterization of the plates was performed by means of optical microscopy and infrared (IR) absorption spectroscopy. Birefringence images were taken using a binocular with a polarization attachment. The IR spectra were measured with a Bruker Vertex 70 FTIR spectrometer using a circular aperture approximately 3 mm in diameter. The type and concentrations of nitrogen defects in the diamond plates were determined from the infrared spectra using standard procedures (Zaitsev, 2001). It was found that the plates contained nitrogen impurities predominantly in the form of isolated substitutional atoms (C-centers, type-Ib) with concentrations in the range 100–150 ppm.

A preliminary characterization of the diamond plates was made by Bragg topography with a polychromatic X-ray beam provided by the liquid Ga point laboratory source and by polarization optical microscopy. A high-resolution study of the diamond-plate quality was carried out by measuring RCI at the PETRA III P01 beamline of the Deutsches Elektronen–Synchrotron (DESY) (Wille *et al.*, 2010). The samples were studied at room temperature in Bragg geometry using a
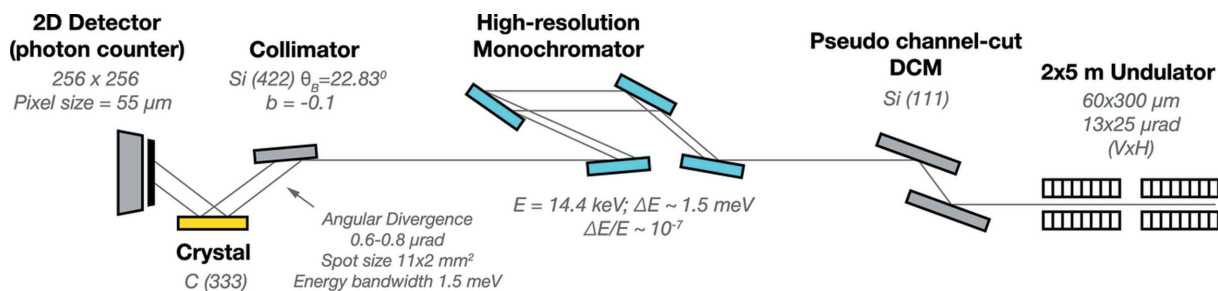
Figure 1
Setup for high-resolution RCI of the diamond (333) reflection at an energy of E = 14.41 keV. It includes two 5 m undulators, an Si pseudo channel-cut double-crystal monochromator, a four-crystal high-resolution Si(400) (10,6,4) monochromator, an asymmetrically cut silicon (422) collimator, the sample and the 2D detector.

monochromatic collimated beam at 14.41 keV energy. The setup includes a high-resolution Si(400) (10,6,4) monochromator that provides $\Delta E/E = 10^{-7}$ and asymmetric Si(422) reflection which works as the collimator with asymmetry parameter $b = -0.1$. The beam impinging on the studied diamond plates has an energy bandwidth of 1.5 meV, angular divergence of 0.6–0.8 µrad and spot size full width at half-maximum (FWHM) of 11 mm × 2 mm along and perpendicular to the reflection plane, respectively. RCI was performed by angular scanning of the studied crystals with a step size of 0.17 µrad using a 2D photon-counting Lambda detector (X-Spectrum) with 55 µm pixel size and 256 × 256 pixel total area. The experimental setup is shown in Fig. 1. The rocking curves were analyzed for each pixel and the maps of the FWHM and center of mass (COM) of reflection were obtained. The setup was tested using a good quality Si(555) reflection with a theoretical width of reflection of 1.46 µrad. The mean reflection FWHM obtained for all pixels was 1.60 µrad, giving an incoming beam divergence of 0.65 µrad. The integral reflection FWHM was 1.70 µrad indicating an ~0.4 µrad spread of the beam direction over the entire spot size.

For the RCI we have chosen a high-order (333) reflection of diamond because of (i) the beam incidence angle, which is ~45° to the sample, whereas the Bragg angle for the (333) plane is 38.84°, so that mounting the system, which can introduce strains to the plate, is not required; and (ii) high sensitivity to small lattice distortions as a result of the narrow rocking curve with a theoretical width of 2.13 µrad (0.46 arcsec).

3. Results and discussion

Preliminary analysis of the diamond plate quality was carried out using optical polarization microscopy and Bragg topography on a polychromatic Ga $K\alpha$ (9.2 keV) laboratory source. The (111) reflections were registered on a high-resolution CCD detector (Rigaku) with a pixel size of 2.16 µm. Crystal (1) demonstrates a number of defects at the corners, related to the cutting process and dislocations near the edges (Fig. 2). On the microscopy image at the central part we can see the area with extended defects. These defects are not
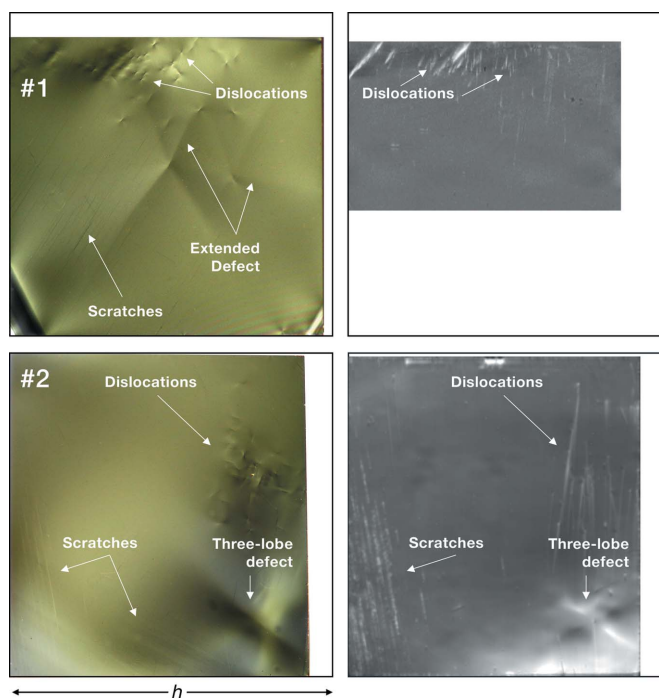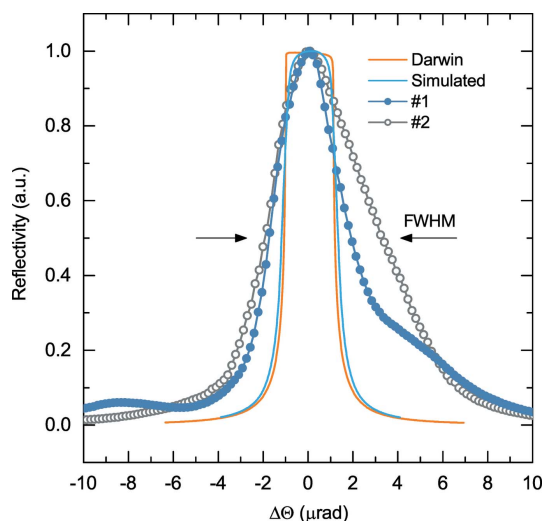

Figure 2
Optical polarization microscopy (left) and Bragg topography (right) images for both diamond plates (h denotes the 3.5 mm scale).

visible in the X-ray topography image due to the small extinction depth of X-rays for the (111) reflection: 2.23 µm, whereas optical microscopy reveals all the defects throughout the plate thickness. The area at the bottom-right part of the crystal is dislocation-free and 1.7 mm × 1.6 mm in size.

Crystal (2) exhibits similar features with dislocations close to the one edge of the plate, a three-lobe defect at one of the corners and scratches on the surface. This crystal demonstrates a larger 1.8 mm × 2.3 mm dislocation-free area.

The integral rocking curves (RCs) from the overall area obtained by the high-resolution RCI are shown in Fig. 3 together with theoretical Darwin curves. The theoretical curve for a diamond (333) reflection at 14.41 keV has an FWHM of 2.13 µrad for the monochromatic and collimated beam and has an FWHM of 2.53 µrad for the current setup considering the beam divergence and the energy dispersion. The FWHM

Figure 3
Integral rocking curves of the diamond crystal plates. The experimental FWHM values are much higher than the theoretical ones (Darwin) and the simulated curve, which considers the beam divergence and energy dispersion of the setup.

values for the crystals studied were found to be 3.65 µrad and 5.23 µrad for crystals (1) and (2), respectively. The broadening of the RCs shows a significant influence of the dislocations and strain on the crystal quality.

Rocking curve maps representing FWHM and COM values are shown in Fig. 4. FWHM maps show the perfection of the crystal lattice and the COM indicates the presence of strain in the crystal. The FWHM map of crystal (1) shows variation from 1.9 µrad up to 5.2 µrad. The effect of RC-narrowing is observed at the bottom-left corner and around dislocation regions. We should note that FWHM values in the range 3–3.5 µrad are related to the strain induced by polishing, whereas values above 3.5 µrad are related to the defects and dislocations in the crystals. The COM variation in the dislo-

cation-free area falls within 1.15 µrad. The deviation of COM values due to defects and dislocations reach 10 µrad and 4 µrad, respectively. Comparison of the RCI maps with the optical microscopy image reveals the presence of extended defects close to the center of the crystal. The difference between an X-ray topography image and an RCI here can be explained by the extinction depth, which is 2.23 µm for the (111) reflection and 16.49 µm for the (333) reflection. The higher-order reflection allows us to discover features related to in-depth defects.

The FWHM distribution of crystal (2) is similar to crystal (1) with values ranging from 1.9 µrad to 5.6 µrad. Excessive broadening of the RCs above 5.2 µrad can be attributed to the presence of the three-lobe defect. In this crystal, COM distribution in the defect-free area is higher compared with crystal (1), falling within 1.49 µrad. Note the COM distribution shows that the surface is curved or non-uniformly strained, limiting the working area.

To check the crystalline quality in detail we compared the RCs from the different parts of the diamond crystals. The points were chosen as follows: from the central part of the crystal (point 1), from a pronounced defect (point 2) and from the part with the smallest FWHM (point 3).

Crystal (1) demonstrates a symmetrical rocking curve at point 1 with an FWHM value of 2.56 µrad, which is almost equal to the theoretical value [Fig. 5(a)]. The shape of the curve is uniform, without extra broadening, slope change or wings. The curve from point 2 is symmetrical at the bottom and demonstrates peak-splitting with an FWHM of 3.57 µrad. This region in the crystal possesses strains caused by polishing. Narrowing of the rocking curve (FWHM = 1.97 µrad) from point 3 can be described by small distortions in a crystal cell, an overall mosaicism and curved surface leading to a multiple diffraction effect (Chang, 1987).

The RC from point 1 of crystal (2) is narrow, with an FWHM of 2.40 µrad [Fig. 5(b)]. The result obtained from
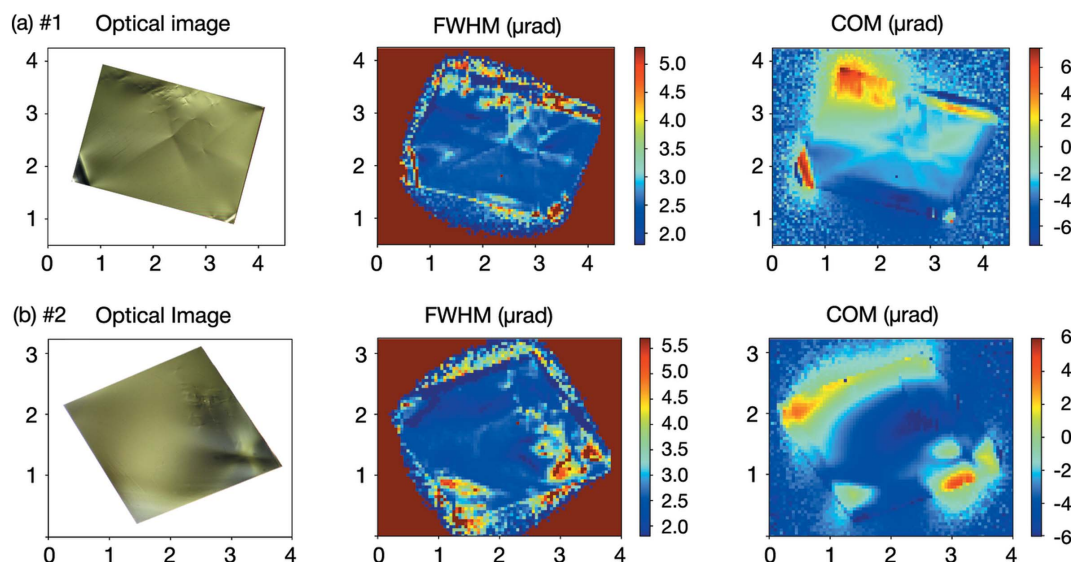
Figure 4
RCI maps for crystals (a) (1) and (b) (2) compared with optical imaging. The labels are presented in millimetres.

Table 1
Size and characteristics of the diamond plates derived from the RCI.

θ and $\delta\theta_{\mathrm{FWHM}}$ are the FWHM values and standard deviation. $\delta\theta_{\mathrm{COM}}$ values show the standard deviation of the COM map.

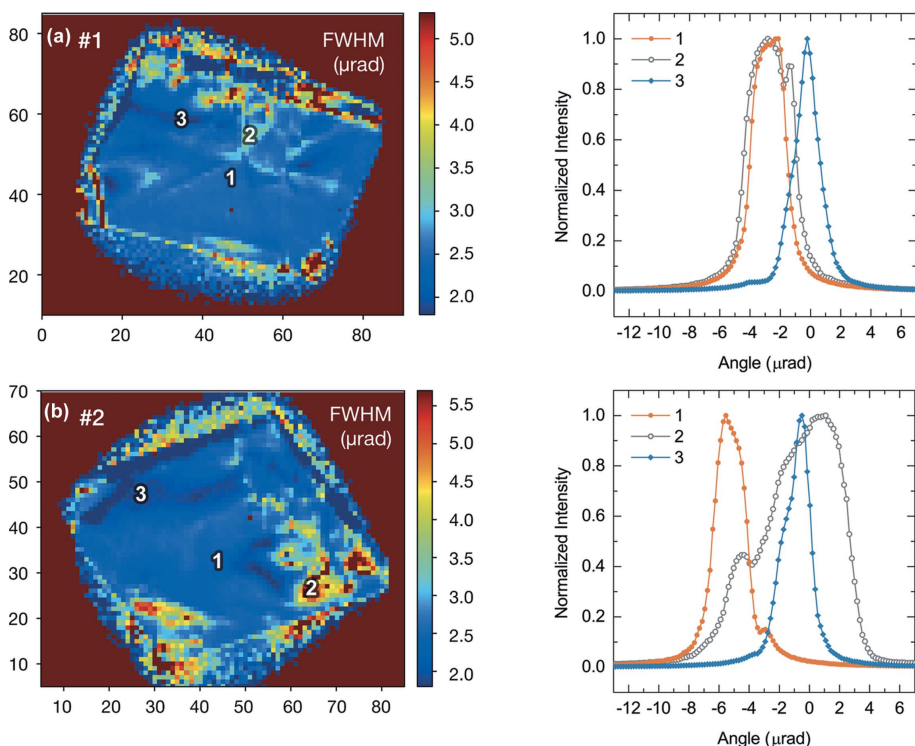| Crystal number	Size (mm)	Miscut angle (°)	θ_{RMS} (µrad)	$\delta\theta_{\mathrm{FWHM}}$ (µrad)	$\delta\theta_{\mathrm{COM}}$ (µrad)	Working area (mm)	Working area integral FWHM (µrad)	Working area $\theta_{\mathrm{FWHM}} \le 3$ µrad (mm)
1	3.4 × 3.2	3.67	2.60	0.38	1.15	1.0 × 2.2	2.93	1.5 × 2.8
2	2.9 × 3.1	6.06	2.64	0.45	1.49	1.0 × 1.6	3.33	1.4 × 1.7

Figure 5
FWHM maps and rocking curves corresponding to the indicated pixels for the diamond plates of crystals (a) (1) and (b) (2). The pixels were taken from the central area (point 1), defect (point 2) and the lowest FWHM value (point 3).

point 2 demonstrates that the defect area cannot be considered as the working area in optical applications. The shape is complex with additional peaks on the left side and broadening of the curve more than two times exceeding the theoretical value. In the narrowest part of the crystal (point 3) the FWHM value is 2.03 µrad, similar to that in the crystal (1). Note that COM values shift by up to 4 µrad, demonstrating strains or crystal curvature.

For a more precise estimation of the working area in the diamond crystals we reduced the range of values at FWHM maps. The areas with dislocations and significant strain represented by values higher than 4.0 µrad were cut. The lowermost values were limited to 1.9 µrad. Considering this, we plotted FWHM maps and made a statistical distribution of FWHM values (Fig. 6). The RMS values and associated standard deviations are 2.60 ± 0.38 µrad and 2.64 ± 0.45 µrad for crystal (1) and (2), respectively. Working areas with a deviation of 0.5 µrad from the theoretical value were estimated as 1 mm × 2.2 mm and 1 mm × 1.6 mm for crystals (1)

and (2), respectively. Extending the deviation value to 1 µrad for less demanding optical applications results in working areas of 1.5 mm × 2.8 mm for (1) and 1.4 mm × 1.7 mm for (2). All of the parameters are presented in Table 1.

As a result, crystal (1) has a larger working area and a lower FWHM mean value and deviation compared with crystal (2), making it more suitable for optical applications. The region around the working area can be used for crystal mounting. Crystal (2) has a threefold defect, which covers around 30% of the surface. The dislocations visible at 10% of the I_{max} map cover another 10% near the defect. The miscut angle of 6.06° together with the polishing process results in a highly strained region at the opposite angle of the plate and overall crystal curvature, resulting in a shift of up to 4 µrad in COM. To avoid the aforementioned features, we need to improve the cutting process to receive a miscut angle <2° and a polishing process to reduce the curvature and additional strains. This will allow us to achieve at least a 2.5 mm × 2.5 mm working area enough for XFEL and fourth-generation source optical applications. Considering the paper by Khokhryakov, where the size of the plate was as high as 6.9 mm × 3.7 mm, one can receive an even larger working area (Khokhryakov et al., 2011).

To confirm the applicability of the marked working areas we made integral RCs and compared them with the simulated curve in Fig. 7. The overall shape of the integral RCs is uniform, without secondary peaks or broad wings at the edges. The FWHM values are 2.93 µrad for (1) and 3.33 µrad for (2), exceeding the experimentally calculated value of 2.53 µrad by 0.4 µrad and 0.8 µrad for crystals (1) and (2), respectively. Crystal (1) is better quality in comparison with crystal (2). It has a larger working area and FWHM values close to the theoretical ones and smaller deviations. The integral RC, which also considers the COM distribution, demonstrates a value higher by 0.4 µrad than the simulated curve, making the crystal suitable for almost all optical applications.
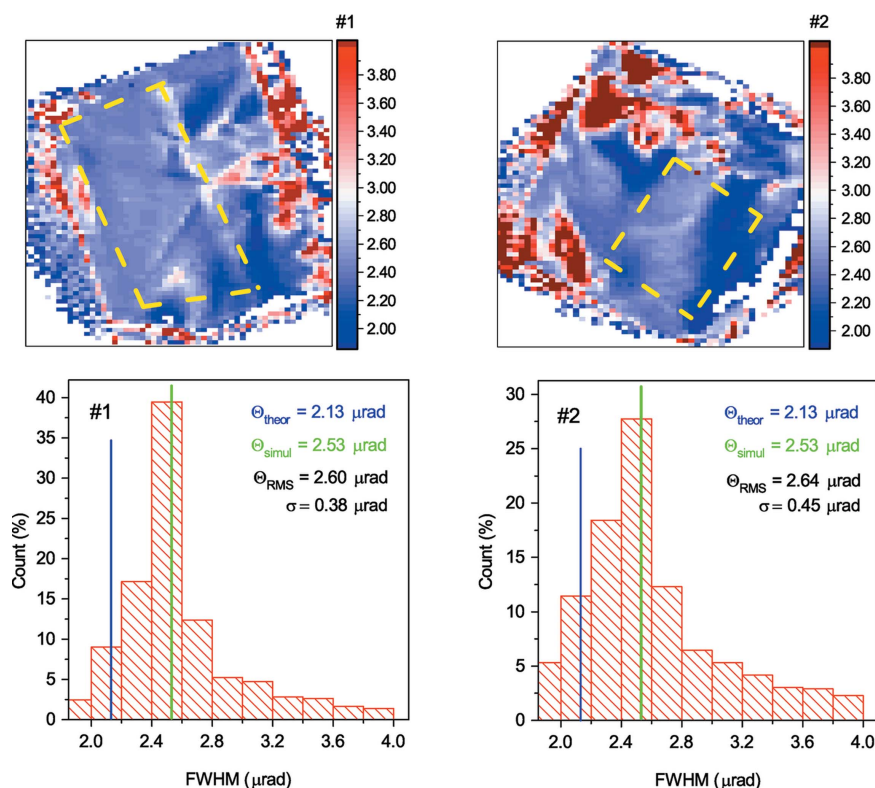
Figure 6
FWHM maps and distribution histograms of diamond plates artificially limited from 1.9 µrad to 4.0 µrad. The data corresponding to defects and highly strained regions due to crystal cut and polishing were removed. The yellow rectangles on the FWHM maps indicate regions that fall within the scope of 1 µrad deviation from the theoretical value. Solid blue lines show the FWHM of the Darwin and simulated curves.
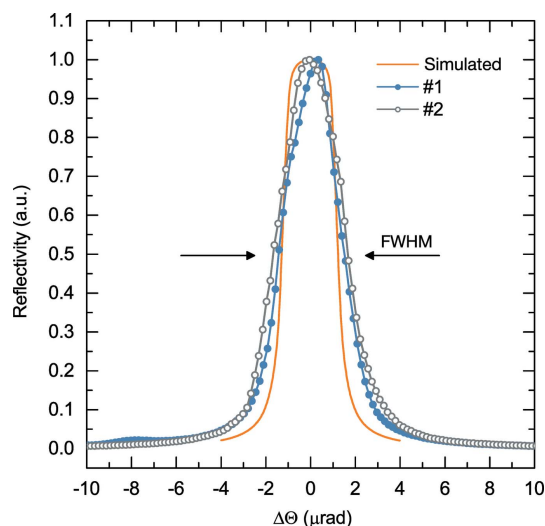
Figure 7
Integral rocking curves taken from the dislocation-free areas indicated in Fig. 6 showing that the deviation of the FWHM falls in the scope of 0.8 µrad

4. Conclusions

In summary we showed that type-Ib (111)-oriented diamond plates can possess a high diffraction quality despite the presence of nitrogen. Two diamond crystals 200 µm-thick with areas of 3 mm^2 were studied by high-resolution RCI. The results demonstrate that the FWHM mean value at the dislocation- and strain-free areas lies within 0.5 µrad deviation from the theoretical value suitable for XFEL and fourth-generation synchrotron source optical applications such as beam splitters and monochromators. The working area of crystal (1) exceeds 50% of the whole crystal surface. Further improvement of the cutting and polishing processes will lead to large Ib diamond crystals (more than 6 mm^2) with larger working areas.

References

Burns, R. C., Chumakov, A. I., Connell, S. H., Dube, D., Godfried, H. P., Hansen, J. O., Härtwig, J., Hoszowska, J., Masiello, F., Mkhonza, L., Rebak, M., Rommevaux, A., Setshedi, R. & Van Vaerenbergh, P. (2009). *J. Phys. Condens. Matter*, **21**, 364224.

Chang, S.-L. (1987). *Crystallogr. Rev.* **1**, 87–184.

Einfeld, D., Schaper, J. & Plesko, M. (1995). *Proceedings of the 1995 Particle Accelerator Conference*, 1–5 May 1995, Dallas, Texas, USA, Vol. 1, pp. 177–179. New York: IEEE.

Grübel, G., Abernathy, D., Vignaud, G., Sanchez del Rio, M. & Freund, A. (1996). *Rev. Sci. Instrum.* **67**, 3349.

Han, Q., Liu, B., Hu, M., Li, Z., Jia, X., Li, M., Ma, H., Li, S., Xiao, H. & Li, Y. (2011). *Cryst. Growth Des.* **11**, 1000–1005.

Hoszowska, J., Freund, A. K., Boller, E., Sellschop, J. P. F., Level, G., Härtwig, J., Burns, R. C., Rebak, M. & Baruchel, J. (2001). *J. Phys. D Appl. Phys.* **34**, A47–A51.

Khokhryakov, A. F., Palyanov, Y. N., Kupriyanov, I. N., Borzdov, Y. M., Sokol, A. G., Härtwig, J. & Masiello, F. (2011). *J. Cryst. Growth*, **317**, 32–38.

Macrander, A. T., Krasnicki, S., Zhong, Y., Maj, J. & Chu, Y. S. (2005). *Appl. Phys. Lett.* **87**, 194113.

Palyanov, Y. N., Borzdov, Y. M., Khokhryakov, A. F., Kupriyanov, I. N. & Sokol, A. G. (2010). *Cryst. Growth Des.* **10**, 3169–3175.

Palyanov, Y. N., Kupriyanov, I. N., Khokhryakov, A. F. & Ralchenko, V. G. (2015). *Cryst. Growth Des.* **11**, 2599–2605.

Polyakov, S. N., Denisov, V. N., Kuzmin, N. V., Kuznetsov, M. S., Martyushov, S. Y., Nosukhin, S. A., Terentiev, S. A. & Blank, V. D. (2011). *Diamond Relat. Mater.* **20**, 726–728.

Sergueev, I., Döhrmann, R., Horbach, J. & Heuer, J. (2016). *J. Synchrotron Rad.* **23**, 1097–1103.

Shvyd'ko, Y., Blank, V. & Terentyev, S. (2017). *MRS Bull.* **42**, 437–444.

Stoupin, S. (2014). *Diamond Relat. Mater.* **49**, 39–47.

research papers

Stoupin, S., Antipov, S., Butler, J. E., Kolyadin, A. V. & Katrusha, A. (2016). *J. Synchrotron Rad.* **23**, 1118–1123.

Sumiya, H., Harano, K. & Tamasaku, K. (2015). *Diamond Relat. Mater.* **58**, 221–225.

Sumiya, H. & Satoh, S. (1996). *Diamond Relat. Mater.* **5**, 1359–1365.

Theveneau, P., Baker, R., Barrett, R., Beteva, A., Bowler, M. W., Carpentier, P., Caserotto, H., De Sanctis, D., Dobias, F., Flot, D., Guijarro, M., Giraud, T., Lentini, M., Leonard, G. A., Mattenet, M., McCarthy, A. A., McSweeney, S. M., Morawe, C., Nanao, M., Nurizzo, D., Ohlsson, S., Pernot, P., Popov, A. N., Round, A., Royant, A., Schmid, W., Snigirev, A., Surr, J. & Mueller-Dieckmann, C. (2013). *J. Phys. Conf. Ser.* **425**, 012001.

Wille, H. C., Franz, H., Röhlsberger, R., Caliebe, A. & Dill, F. U. (2010). *J. Phys. Conf. Ser.* **217**, 012008.

Yabashi, M., Goto, S., Shimizu, Y., Tamasaku, K., Yamazaki, H., Yoda, Y., Suzuki, M., Ohishi, Y., Yamamoto, M. & Ishikawa, T. (2007). *AIP Conf. Proc.* **879**, 922–925.

Zaitsev, A. M. (2001). *Optical Properties of Diamond*. Berlin, Heidelberg: Springer.